Zus, F., Grzeschik, M., Bauer, H. S., Wulfmeyer, V., Dick, G., Bender, M. (2008): Development and optimization of the IPM MM5 GPS slant path 4DVAR system. - Meteorologische Zeitschrift, 17, 6, 867-885

DOI: 10.1127/0941-2948/2008/0339

Meteorologische Zeitschrift, Vol. **17**, No. 6, 867-885 (December 2008)

Article

Development and optimization of the IPM MM5 GPS slant path 4DVAR system

FLORIAN ZUS[1*], MATTHIAS GRZESCHIK[1], HANS-STEFAN BAUER[1], VOLKER WULFMEYER[1], GALINA DICK[2] and MICHAEL BENDER[2]

[1]Institut für Physik und Meteorologie, Universität Hohenheim, Stuttgart, Germany
[2]HelmholtzZentrum Potsdam, GeoForschungsZentrum, Potsdam, Germany

(Manuscript received April 4, 2008; in revised form October 3, 2008; accepted October 3, 2008)

Abstract

This article describes the development of tools for routine 4-dimensional variational data assimilation of Global Positioning System Slant Total Delay (STD) data in the framework of the MM5 system at the Institute of Physics and Meteorology of the University of Hohenheim. The Slant Total Delay forward operator is introduced which allows model validation and the assimilation in the Message-Passing Interface environment. An experiment is conducted which highlights the importance of accurate model physics in the variational assimilation system. We demonstrate that the model minus observation statistics of STD data crucially depends on the convection scheme and the implementation of horizontal diffusion. A set of modifications to the existing non linear, tangent linear and adjoint model is presented. These include an improvement of the horizontal diffusion scheme and the implementation of the Grell cumulus convective scheme in order to eliminate the observed systematic tendency in the model minus observation statistics of the STD data and precipitation in mountainous terrain. A first assimilation experiment with the improved MM5 variational assimilation system shows promising results.

Zusammenfassung

Dieser Artikel beschreibt die Entwicklung von Tools zur 4-dimensionalen variationellen Assimilation von Global Positioning System Slant Total Delay (STD) Daten mit dem MM5 System am Institut für Physik und Meteorologie der Univerität Hohenheim. Der Vorwärtsoperator wird vorgestellt, der Validationsstudien und die Assimilation in die Message-Passing Interface Umgebung des MM5 erlaubt. Wir demonstrieren, dass die Modell-minus-Beobachtung-Statistik der STD Daten entscheidend von dem verwendeten Konvektionsschema und der Implementierung der horizontalen Diffusion abhängt. Ein Satz von Modifikationen zum existierenden nicht-linearen, tangent-linearen und adjungierten Modell wird präsentiert. Ein verbessertes Schema der horizontalen Diffusion und die Implementierung des Konvektionsschemas von Grell sind notwendig, um die systematische Tendenz in der Modell-minus-Beobachtung-Statistik der STD Daten und des Niederschlags in komplexen Gelände zu vermeiden. Ein erstes Assimilationsexperiment zeigt vielversprechende Ergebnisse.

1 Introduction

During the last few years, considerable progress has been achieved in numerical weather prediction (NWP) of mesoscale gamma atmospheric phenomena. This progress is largely due to a better understanding of small-scale processes, a rapid growth in computer power, permitting a significant increase in model resolution, as well as the availability and assimilation of observations. Recent results in nowcasting and short-range weather forecasting demonstrate that variational data assimilation in combination with high-resolution modeling is a promising approach for improving the quality of Quantitative Precipitation Forecasting (QPF) on the mesoscale (ZOU et al., 1995; XIAO et al., 2005; WULFMEYER et al., 2006; SAITO et al., 2006).

Here we focus on the assimilation system that has excellent potential to exploit the maximum information content of various observing systems with high temporal resolution: four-dimensional variational assimilation (4DVAR). This can be explained by the fact that the 4DVAR takes into account the dynamics of the atmosphere as well as the background and observation errors in a consistent manner. Notably, the 4DVAR is equivalent to a full rank extended Kalman Filter (EKF) over the data assimilation window. For a discussion of pros and cons of various assimilation schemes see e.g. BOUTTIER and COURTIER (1999); KALNAY et al. (2007); GUSTAFSSON (2007).

The availability of precise and continuous observations related to water vapor is crucial. Although ground-based techniques such as radiosondes, water-vapor radiometers or lidar systems (BEHRENDT et al., 2002; WULFMEYER et al., 2003) are sensitive to the water vapor content in the atmosphere, they are currently not available in dense networks with high temporal resolution. Radiosondes for example are launched typically only twice a day and they are sparse over wide areas. Due to their low cost and high rate, GPS (Global Posi-

*Corresponding author: Florian Zus, Institut für Physik und Meteorologie, Universität Hohenheim, Garbenstrasse 30, 70599 Stuttgart, Germany, e-mail: Florian.Zus@uni-hohenheim.de

DOI 10.1127/0941-2948/2008/0339

0941-2948/2008/0339 $ 8.55

tioning System) receivers can be assembled into dense networks with high temporal resolution.

The radio signals used by GPS are changed in a characteristic way when they pass through the Earth's atmosphere. The tropospheric delays which are caused by the signal refraction in the electrically neutral (or non-ionised) atmosphere can be considered as meteorological observations containing signatures of the atmospheric humidity field. They are the basis for the concept known as GPS meteorology (BEVIS et al., 1992; WICKERT and GENDT, 2006). One distinct advantage of GPS ground based measurements compared to other satellite observations is that it provides data in all weather conditions, i.e. the measurements are not affected by clouds. As water vapor is often under-observed both in time and space during active weather, this capability of the GPS data is expected to improve the skill of short range predictions of medium to heavy rainfall systems. The high temporal resolution of GPS ground-based measurements can be used for model validation and data assimilation (CUCURULL et al., 2000; POLI et al., 2007) or detailed studies of the structure in water-vapor fields (HAAN et al., 2002). To date, most of the ground-based GPS data assimilation studies have been conducted using the Zenith Total Delay (ZTD) or Integrated Water Vapor (IWV) estimates (VEDEL and HUANG, 2004; VEDEL and SATTLER, 2006). It is found that data assimilation of ZTD data has a weak but positive impact on the NWP forecasts of humidity and precipitation.

HA et al. (2003) performed a series of observing system simulation experiments to assess the impact of slant wet delays on the short-range prediction of a squall line. Slant wet delay data from a hypothetical network of ground-based GPS receivers were assimilated using the MM5 4DVAR system. It was demonstrated that the assimilation of slant wet delays results in significant changes in moisture, temperature and wind fields. These changes led to a stronger surface cold front and stronger convective instability ahead of the front. Consequently, the assimilation of slant wet delay produced a considerably improved six hour forecast of a squall line, in terms of rainfall prediction and mesoscale frontal structure. In order to assess the additional value of slant wet delay assimilation (as compared with zenith wet delay), a parallel experiment in which precipitable water was assimilated was performed. The assimilation of slant wet delays was superior in recovering water vapor information between receiver sites and in short-range precipitation forecast, both in terms of rainfall distribution and intensity, and retrieved more accurately the temperature and moisture structure in the convectively unstable region.

Recently, JÄRVINEN et al. (2007) analyzed the data assimilation of hypothetical and real STD (Slant Total Delay) observations in the framework of the HIRLAM (High-Resolution Limited Area Modeling) 3DVAR (3-dimensional variational assimilation) system. The experiments with hypothetical data showed that their assimilation results in reasonable specific humidity analysis increments. Since one of the main benefits of STD observations is their ability to capture fine-scaled asymmetric humidity structures present in the atmosphere (ERESMAA et al., 2007), the assimilation system was able to reproduce the asymmetric information content in the hypothetical observations. Real STD observations were assimilated for an arbitrary single case and the resulting specific humidity analysis increments were found to have a similar structure to those obtained with a comparable radiosonde or ZTD observing network.

While the results presented so far indicate that the measurements from ground-based GPS networks are highly valuable for short range prediction of precipitation, it is important to recognize that the assimilation of observations related to water vapor in a convective and/or pre-convective environement is highly challenging. One major difficulty is the accuracy of model physics. In particular, the convection parameterization used in the data assimilation can be regarded as an issue. The problem associated with the convection parameterization scheme is twofold: It is a crude representation of convection and these schemes contain numerous discontinuities which can increase linearization errors leading to adverse effects in 4DVAR (ZUPANSKI, 1993). Beside model physics, deficiencies in model numerics can be substantial (ZÄNGL, 2004b,c).

Prior to any data assimilation efforts, systematic model errors must be identified, quantified and removed. However, it is very difficult to separate the contribution of errors due to initial fields and model parameterizations. A close inspection of a long time series of the model minus observation statistics is one strategy to identify model errors. Corresponding research is the subject of several ongoing projects of the World Weather Research Program (WWRP) such as the Research and Developement Project Convective and Orographically-induced Precipitation Study (COPS). This study will provide a comprehensive set of observations for testing hypotheses on the improvement of QPF in regions with complex terrain including various data assimilation studies (WULFMEYER et al., 2008). For further information on WWRP activities the reader is referred to www.uni-hohenheim.de/cops/ and www.wmo.ch/pages/prog/arep/indexen.html.

Improvements of forecasts can only be expected if progress is made in three areas simultaneously: Handling of problems related to model numerics such as treatment of the governing equations in complex terrain, the improvement of parameterization schemes, and the optimization of initial conditions. In this study, we address these issues by taking advantage of the high temporal resolution STD data. In a first step, we study the performance of model numerics and model physics without any assimilation effort by statistical comparison with STD data. In particular, we focus on the implemen-

tation of horizontal diffusion in complex terrain and the convection parameterization. In a second step, we study the impact of the STD data with the improved physics and numerics within a 4DVAR framework.

This article is organized as follows: In section 2, the MM5 4DVAR system is introduced. The STD forward operator used for both model validation and assimilation is described. In section 3, problems encountered in model physics are discussed and a set of modifications to the existing MM5 4DVAR system is presented. In section 4, a real world application of the improved STD 4DVAR system in a single case experiment is analyzed. A summary and the main conclusions are given in Section 5.

2 Technical introduction

2.1 The MM5 Model

An overview of the MM5 is given in GRELL et al. (1995). The MM5 tangent linear and adjoint modelling system are described in ZOU et al. (1997). A detailed introduction to the MM5 4DVAR system used in this study can be found in RUGGIERO et al. (2001). The 4DVAR system is based on MM5 version 3 (MM5v3). The parallelization was implemented so that the same source architecture for the serial and parallel versions of the code was maintained. RUGGIERO et al. (2002) described the successful development and testing of the MM5v3-based tangent-linear model. Its coding implementation followed the same design as the forecast model. NEHRKORN et al. (2002) succesfully developed and tested the MM5v3-based adjoint model.

The adjoint model contains the same set of physics parameterizations that are in the serial MM5 version 1 (MM5v1) based 4DVAR system. This includes the KUO (1974) convective parameterization, a moist stable precipitation scheme, a simple radiative cooling scheme and a bulk planetary boundary layer (PBL) parameterization. To allow the use of a greater number of vertical levels than is practical with the single-level bulk PBL scheme, the user is given the option to run the MRF (Medium Range Forcast) PBL scheme of HONG and PAN (1996).

2.2 The 4DVAR system

The 4DVAR algorithm allows observations to be assimilated in their raw form at any given point in time and space (BOUTTIER and COURTIER, 1999). The model solution is required to fit the observations in a least-square sense. The minimum of the following cost function J, measuring the difference between the model solution and observations, is determined

$$J[\mathbf{x_0}] = (\mathbf{x}_0 - \mathbf{x}_b)^T \mathbf{B}^{-1} (\mathbf{x}_0 - \mathbf{x}_b) + \sum_{n=0}^{m} (H[\mathbf{x}_n] - \mathbf{y}_n)^T \mathbf{R}^{-1} (H[\mathbf{x}_n] - \mathbf{y}_n) \quad (2.1)$$

where $\mathbf{x}_0$ denotes the analysis vector, $\mathbf{x}_b$ is the background vector and $\mathbf{y}_n$ denotes the observation vector at time n. The model forecast vector $\mathbf{x}_n$ at time n is predicted by the (non-linear) forecast model M, i.e. $\mathbf{x}_n = M...M[\mathbf{x_0}]$. H represents the observation operator which transforms model variables into observation space, and $\mathbf{R}$ denotes the observational error covariance matrix. The analysis vector of the MM5 4DVAR system used in this study consists of the following model control variables: the horizontal wind components, the temperature, the water-vapor mixing ratio, the pressure perturbation and the vertical velocity. Cloud water, cloud ice, surface variables, and the variables at lateral boundaries are not included.

The MM5 4DVAR system only constructs diagonal background error covariance matrices $\mathbf{B}$. This approximation has proven to work well with most studies conducted with the system (ZOU et al., 1995; HA et al., 2003; WULFMEYER et al., 2006; GRZESCHIK et al., 2008). This can be explained by the ability of the 4DVAR to self-generate physically consistent structure functions during model integration (FISHER, 2001). For each control variable, the diagonal elements of $\mathbf{B}$ were specified by constructing the differences between a short-range forecast of 15 minutes and the initial values at each grid point. At each vertical level, the maximum value of the difference is found and assigned to all grid points on that level. This creates a vertical profile of forecast errors valid at all geographical locations of the model. The forecast errors are then squared to produce the diagonal elements of the background error covariance matrix $\mathbf{B}$. There is also an option in the MM5 4DVAR system to prescribe the background error variances from the tables published by PARRISH and DERBER (1992). Theses tables contain the observational errors used for the radio-sounding assimilation in the National Centers for Environmental Prediction spectral statistical interpolation global analyses system at the time of the publication. We experimented with both options and have not found any significant differences yet, since the order of magnitude of the background errors variances were similiar.

Since MM5 is a regional model, it requires an initial condition as well as lateral boundary conditions. To produce lateral boundary conditions, gridded data is needed to cover the entire time period the model is integrated over. For our experiments, the ECMWF (European Centre for Medium range Weather Forecasting) operational analysis was interpolated to the horizontal and vertical resolution used in MM5.

2.3 The STD forward operator and the assimilation system

2.3.1 The STD forward operator

The introduction of a new observation type into the MM5 4DVAR system requires the development of the

observation operator, the adjoint operator and the estimation of the observation error statistics. An STD is an integrated measurement and can be determined with the following equation:

$$STD = \int_R^S \left(k_1 \frac{P}{T} + k_2 \frac{e}{T^2} \right) ds \qquad (2.2)$$

Here P represents the pressure, T the temperature, and e the water-vapor pressure. The constants are given by $k_1 = 77.6$ K/hPa and $k_2 = 3.73 \times 10^5 K^2/$ hPa (WARE et al., 1997; WICKERT and GENDT, 2006). The first term of the integral is known as the slant dry delay SHD and the second part as the slant wet delay SWD. The integration is carried out along the slant path s from the ground based GPS receiver R to the satellite S in question. With an elevation angle at the GPS receiver above 20 degrees, the bending of the ray path through the Earth's atmosphere can be neglected and the STD can therefore be evaluated along a straight line. For a discussion of the accuracy of the line-of-sight assumption the reader is referred to ERESMAA and JÄRVINEN (2004). The GPS coordinates are provided with respect to the IGb2000 reference frame www.ngs.noaa.gov/CORS/Coords.html. The ellipsoidal heights of the GPS receivers are converted to the geoidal heights on top of the determination of the signal path in model grid point space. For details on the undulation, the reader is referred to http://earth-info.nga.mil/GandG/. In the signal path determination, the geoid is treated as a sphere with a mean radius of $R_E = 6370$ km according to the MM5. The Gauss-Lobatto quadrature formula (see e.g. ABRAMOWITZ and STEGUN, 1972) is used to evaluate the integral numerically in model grid point space. The observation operator consists of three components:

In a first step, the geographical location (longitude, latitude, and height above sea level) of the supporting points and the weighted line elements are determined along the signal path from the GPS receiver to the model top. In the second step, pressure, temperature, and water-vapor mixing ratio at the quadrature points are reconstructed. Since in a terrain following sigma coordinate system grid points of the same level do not have the same height, in order to avoid systematic errors, we use a 12-point comprehensive tri-directional interpolation of the model variables at adjacent model grid points. The reconstruction of variables at quadrature points consists of a vertical interpolation followed by a horizontal interpolation using low order piecewise Lagrange polynomials. Close to the ground, the vertical interpolation of water vapor mixing ratio and temperature is limited to the height of the underlying model topography. If more grid points are involved in the interpolation scheme, information spreading in the assimilation is enhanced, but higher-order polynomials can introduce extreme values. In the third step, at each supporting point, the integrand is calculated and the summation is carried out.

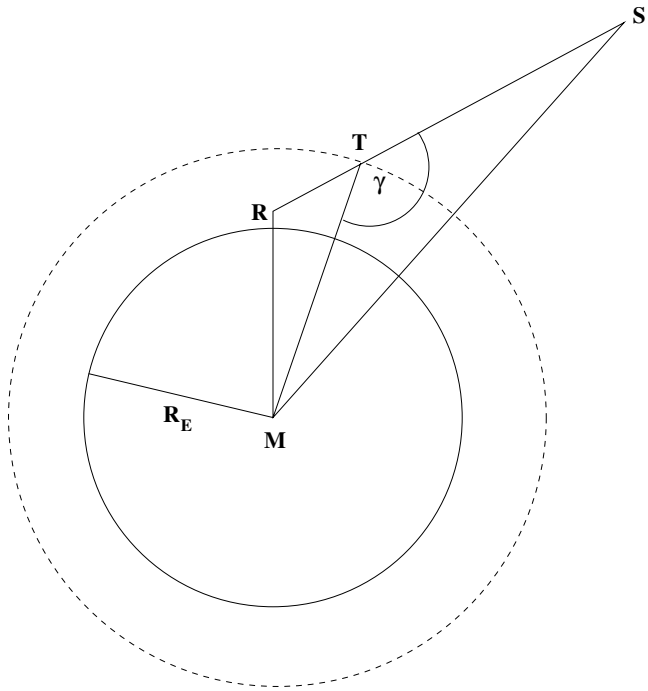

Figure 1: Sketch of the geometry for computing the contribution to the STD above the model top: The GPS receiver is marked with R. The enclosing angle of the direction vector pointing from the model top point T (with height H) to the satellite S and the direction vector pointing from the model top point to the center of gravity M is marked with γ. The signal path above the model top is defined by s and h denotes the integration variable. The radius of the Earth is R_E. The relevant distances are $\overline{MT} = H + R_E$, $\overline{MS} = h + R_E$ and $\overline{TS} = s$.

The number of supporting points m in the numerical integration is increased until a predefined accuracy δ is reached: $|STD_m - STD_{m+1}| < \delta$. In the following simulations, the number of supporting points is fixed and chosen to be 42, which led to sub-millimeter accuracy over the entire elevation range, i.e. $\delta < 1$ mm. In the zenith case, this error converts to about $1/6$ mm in IVW which is sufficiently small as compared to an observation error of about 1 mm in the IVW (DICK et al., 2001). With an average height of the lowest model half sigma level of 63 m, 36 terrain following model layers, and a model top located at 100 hPa, the weights of the endpoints of the quadrature rule are about 8 m at an elevation angle of 90 degree and about 13 m at an elevation angle of 20 degree.

The STD above the finite model top is dealt with separately. The local variability of pressure, temperature, and gravity with geographical latitude and longitude above the model top is neglected. Figure 1 provides a sketch of the geometry of the calculation. We transform the integration variable from the slant path s to the height above sea level h. The law of cosine leads to

$$\begin{aligned} s(h) &= (H + R_E)cos(\gamma) \qquad (2.3) \\ &+ \sqrt{(h + R_E)^2 - (H + R_E)^2 sin(\gamma)^2} \end{aligned}$$

where H denotes the height above sea level of the model top point and γ denotes the enclosing angle of the direction vector pointing from the model top point to the satellite and the direction vector pointing from the model top point to the center of gravity. The derivative of the signal path element with respect to height s' is therefore given by

$$s'(h) = \left[1 - \frac{(H+R_E)^2}{(h+R_E)^2} sin(\gamma)^2\right]^{-0.5} \qquad (2.4)$$

The contribution of the slant total delay above the model top is now determined with aid of the hydrostatic equation and the extended first mean value theorem of integral calculation:

$$\begin{aligned} TOP &= k_1 R_L \int_{\infty}^{H} \frac{s'(h)}{g(h)} P'(h) dh \qquad (2.5) \\ &= k_1 R_L \frac{s'(\xi)}{g(\xi)} P_t \end{aligned}$$

The gas constant of dry air is $R_L = 278.05$ J kg$^{-1}K^{-1}$ and P_t denotes the pressure predicted by the model at the model top point. The decrease of the gravity with respect to height is $g(h) = g_\theta \, R_E^2/(h+R_E)^2$ where g_θ denotes the gravitational acceleration at the latitude θ of the model top point according to the 1967 Geodetic Reference System Formula. Since the derivative of the pressure with respect to the height P' is not predicted by the model, the height above the geoid ξ, for which Equation 2.5 holds, cannot be determined exactly. An accurate approximation can be made by the substitution of the height above the geoid, which results from the assumption of the STANDARD ATMOSPHERE (1976) above the model top. In the zenith case, this formulation is equivalent and turns out to be as accurate as the well known formulation of SAASTAMOINEN (1972). To provide an error of the forward model we estimate the error introduced above and below the model top separately. In the zenith case Equation 2.5 reads as $TOP = k_1 \, R_L \, P_t / g(\xi)$ and the error associated to the mean gravity computed above the model top can be readily neglected, see e.g. (BOSSER et al., 2007; ELGERED et al., 1991). Since the numerical integration below the model top has sub-millimeter accuracy, we estimate the overall error of the forward model in the zenith case to be of the order of 1 mm. In the slant case, the numerical integration below the model top and the assumptions made above the model top (spherical symmetry of the atmosphere) suggest that the error of the forward model is roughly inversely proportional to the sine of the elevation angle at the GPS receiver.

Although interpolation/extrapolation of model grid point variables to the receiver location is performed, a GPS receiver may not be represented by the model if located far below the model topography. In the following, the simulations are limited to GPS receivers, which are located at an adequate distance to the model topography: the magnitude of the difference between a bilinear interpolation of adjacent topographic model heights and the GPS receiver height does not exceed a threshold of 50 m.

To speed up computation, the current NWP systems are usually implemented on parallel computers such that each processor handles only a geographical sub-area. In the MM5 4DVAR version used in this study this is carried out using parallelization techniques. In principle, it involves using spatial domain decomposition where the horizontal analysis domain is partitioned into smaller subdomains or patches. A separate processor can then be dedicated to the computation for a specific subdomain. During the execution of the 4DVAR code, each patch requires only the boundary information from its neighbouring patches. Communication between various patches is accomplished with the use of the standard MPI environment. At low elevation angles, the signal from the GPS receiver to the satellite can intersect two or more subdomains. Some additional logic is required in the routines when compared to the single processor version: In the forward model integration, the contributions to the STD determined by the processor IDs in question are gathered to compute the total STD and the corresponding normalized departure. In the backward model integration, the update of the adjoint variables is restricted to the processor IDs in question. After appropriate tests, the forward model and the adjoint model were implemented into the MPI environment of the 4DVAR system, so that speedy assimilation of STD data became routinely possible. With a horizontal domain size of 64×70 grid points and 30 processors the speed up factor is about 10 compared to a single CPU.

2.3.2 Quality control and the estimate of the observation error

In the 4DVAR experiments, some medium filtering of the STD data based on the relative departure of the slant wet delay is applied in order to reject questionable data and to avoid problems in the minimization due to large differences between the model prediction and the measurements. If we assume that the slant dry delay is well reproduced by the model, a good estimate of the relative departure of the slant wet delay is given by $r = \delta STD/SWD$ where δSTD denotes the STD model minus observation departure and SWD denotes the slant wet delay predicted by the model. In the first forward model integration of the 4DVAR, we reject all data for which $|r| > 0.2$. As can be seen in the following simulations, this threshold is located at the tail of the Gaussian distribution of the relative departure of the slant wet delay (see Figure 4) and thus will remove potential outliers in the assimilation. This data is also not considered in the following forward and backward model integrations and is therefore permanently black listed during minimization. We did not perform any cross check for spatial and temporal consistency of

the STD data since to date we are not aware of any existing rigorous strategy to do so.

Several studies were undertaken to determine the error of STD data by means of intercomparison with independent observations like water vapor radiometers. However, it remains difficult to estimate the real error of the STD data. An initial comparison of GPS stations in Germany with the high-resolution local model of the German Weather Service (DWD) over more than 200 days gives a standard deviation of about 1 mm in the IVW (DICK et al., 2001) which would convert to a standard deviation of about 6 mm in the ZTD. Note that the determination of both the IVW and the ZTD data from the raw measurement contains numerous assumptions. Further studies using different methods are required. In the absence of more accurate estimates and on the basis of the error of ZTD data provided by GFZ Potsdam, we assume the overall error of a STD to be of the order of a few millimeters (about 1 to 6 mm) times the inverse of the sine of the elevation angle at the GPS receiver. In the following assimilation experiment, we used a uniform observation error of $\sigma(\epsilon) = 3/sin(\epsilon)$ mm where ϵ denotes the elevation angle at the GPS receiver. For simplicity and due to insufficient knowledge of error correlation in the Precise Point Position (PPP) algorithm, we disregard correlation of the STD data. Therefore the observational error matrix which enters the cost function is strictly diagonal.

3 Analysis of the MM5 4DVAR model physics

The underlying hypothesis of 4DVAR is that the model is perfect. The model physics used in a 4DVAR system must be as sophisticated as possible in order to preclude any negative effects. The strategy is to a) identify and b) to remove model errors prior to any data assimilation effort by statistical comparisons of simulated and observed STD data. After the sensitivity study we perform an assimilation experiment with improved physics.

To date we have not been e able to identify two serious deficiencies in the model physics of the MM5 4DVAR system, which become obvious in more or less complex terrain, namely the deep convection scheme and the implementation of the horizontal diffusion. These deficiencies could be identified by screening the model minus observation departure of the high temporal resolution STD data.

To demonstrate the capabilities of the STD data for validation purposes, we carried out model forecasts initialized by an ECMWF analysis valid at 00 UTC on August 14, 2007. The model configuration is summarized in Table 1 (Simulation 1 and 2). The horizontal resolution was 18 km and we use 36 terrain following sigma layers. The model top was located at 100 hPa. For the simulations, the model physics available in the

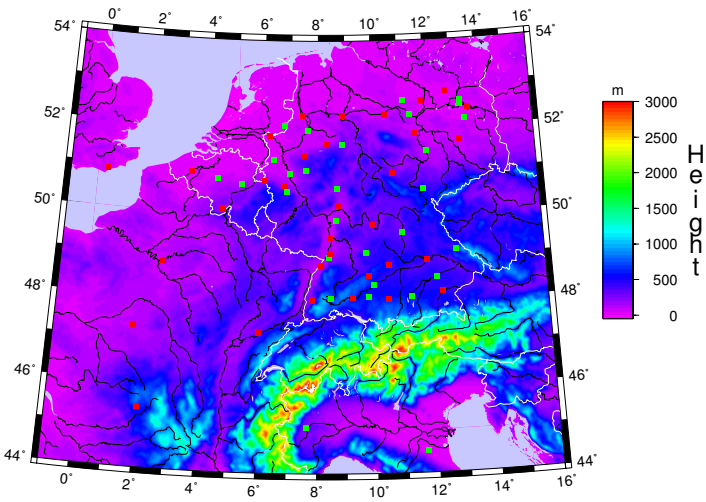

Figure 2: GPS network green and GPS network red providing STD data on August 14, 2007.

MM5 4DVAR was used: the MRF PBL scheme, a simple radiative cooling scheme, a moist stable precipitation scheme and the Kuo cumulus scheme. The two simulations differ by the horizontal diffusion scheme. The simplified physics does not allow a long-range forecast. We limited the model integration to six hours. No spin-up run to remove high frequency waves which may result from the resolution jump from the ECMWF analysis to the MM5 model grid configuration was performed. The resolution jump from the ECMWF analysis to the MM5 model grid configuration is rather small (25 to 18 km) and therefore the spin-up measured (in terms of the mean surface pressure tendency) should be limited but we cannot preclude a possible spin-up effect caused by hydrometeors which are all reset to the initial state.

An overview of the geographical location of the observing GPS network (network red) used in this experiment is given in Figure 2. We evaluated the STD data from 33 GPS receivers distributed over Germany down to an elevation angle of 20 degree with a temporal resolution of 15 minutes.

3.1 Horizontal diffusion

In the MM5 4DVAR, two types of horizontal diffusion are used to control non-linear instability: second-order diffusion is used for the row and column of the grid points next to the lateral boundaries, while the more scale-selective fourth-order diffusion is used in the interior of the domain (GRELL et al., 1995). In analytical form, the fourth-order diffusion F reads:

$$F = -K_h \left(\frac{\partial^4 \alpha}{\partial x^4} + \frac{\partial^4 \alpha}{\partial y^4} \right) \qquad (3.1)$$

where α is any prognostic variable and K_h denotes the diffusion coefficient. The horizontal diffusion operator is applied on constant sigma surfaces, i.e. the discretization is applied in computational space and not, as the

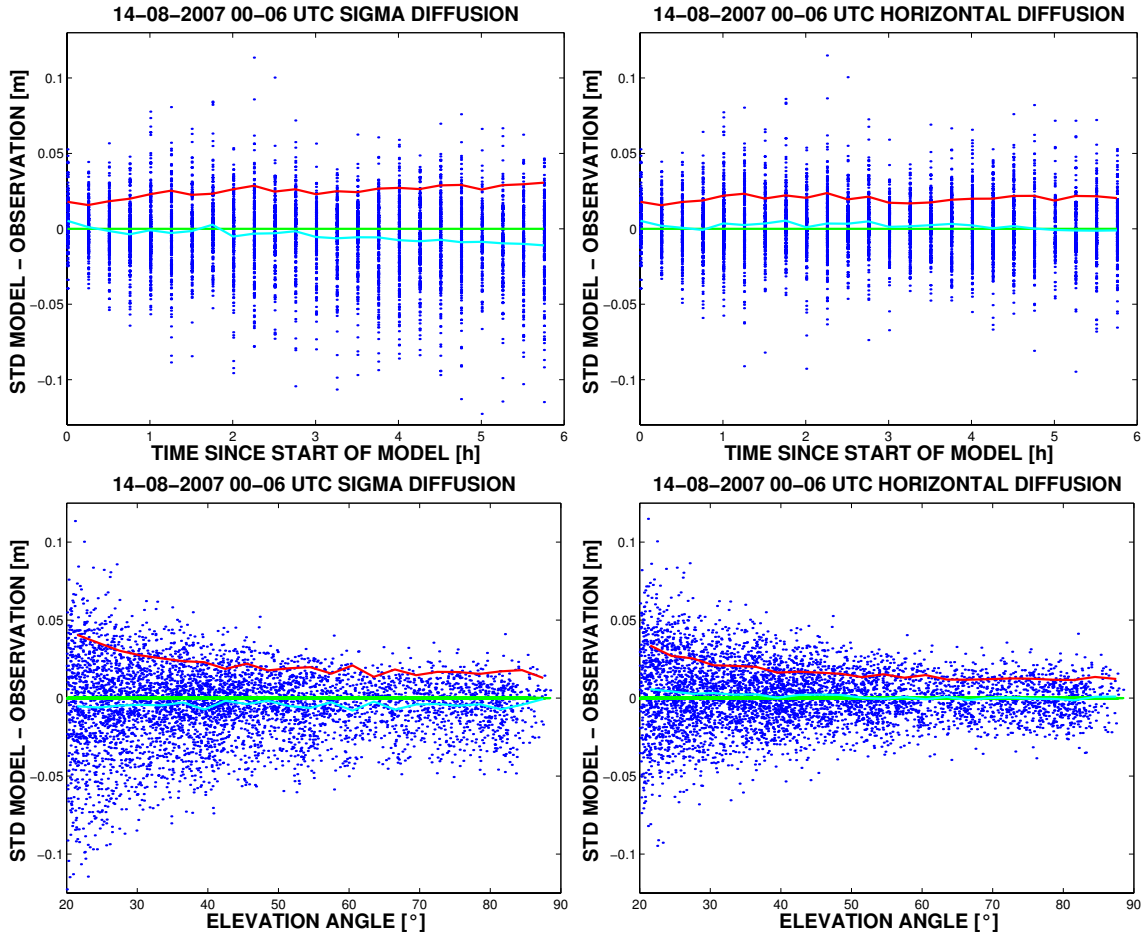

Figure 3: STD model minus observation departure as a function of the time (top) and as a function of the elevation angle (bottom) for sigma diffusion (left) and the modified horizontal diffusion (right). The red line indicates the rms and the cyan line the bias. The green line indicates null bias.

Table 1: Table summarizing the configuration used in the sensitvity study and in the assimilation experiments (August 14, 2007). The simulations (1 and 2) are initialized by the ECMWF analysis valid at 00 UTC. The forecast is either initialized by the ECMWF analysis valid at 00 UTC (reference run) or by the initial state generated by the assimilation experiments.

Configuration	Simulation 1	Simulation 2	Forecast	Assimilation	Assimilation B
Horizontal Resolution	18 km	18 km	18 km	18 km	18 km
Boundary Layer	MRF	MRF	MRF	MRF	MRF
Radiation scheme	simple	simple	simple	simple	simple
Cloud Physics	simple	simple	simple	simple	simple
Horizontal Diffusion	sigma	modified	modified	modified	sigma
Convection scheme	Kuo	Kuo	Grell	Grell	Kuo
GPS data network	red	red	red + green	red	red
GPS data frequency	15 min	15 min	15 min	30 min	30 min
Assimilation window	–	–	–	0–3 UTC	0–3 UTC
Forecast window	0–6 UTC	0–6 UTC	0–6 UTC	–	–

equation above would indicate, in cartesian coordinates. Thus serious errors over mountainous terrain, particulary for atmospheric variables having a strong vertical gradient, like water vapor and temperature, are introduced.

There are currently two options in the MM5 4DVAR for calculating the horizontal diffusion. In the first option, actual temperature is used for computing the diffusion along sigma levels. Second, the perturbation temperature, namely the difference between the actual temperature and a given reference temperature, is used for computing the diffusion along sigma levels. This first option tries to equalize the temperature differences on the terrain following model surfaces, and therefore tends

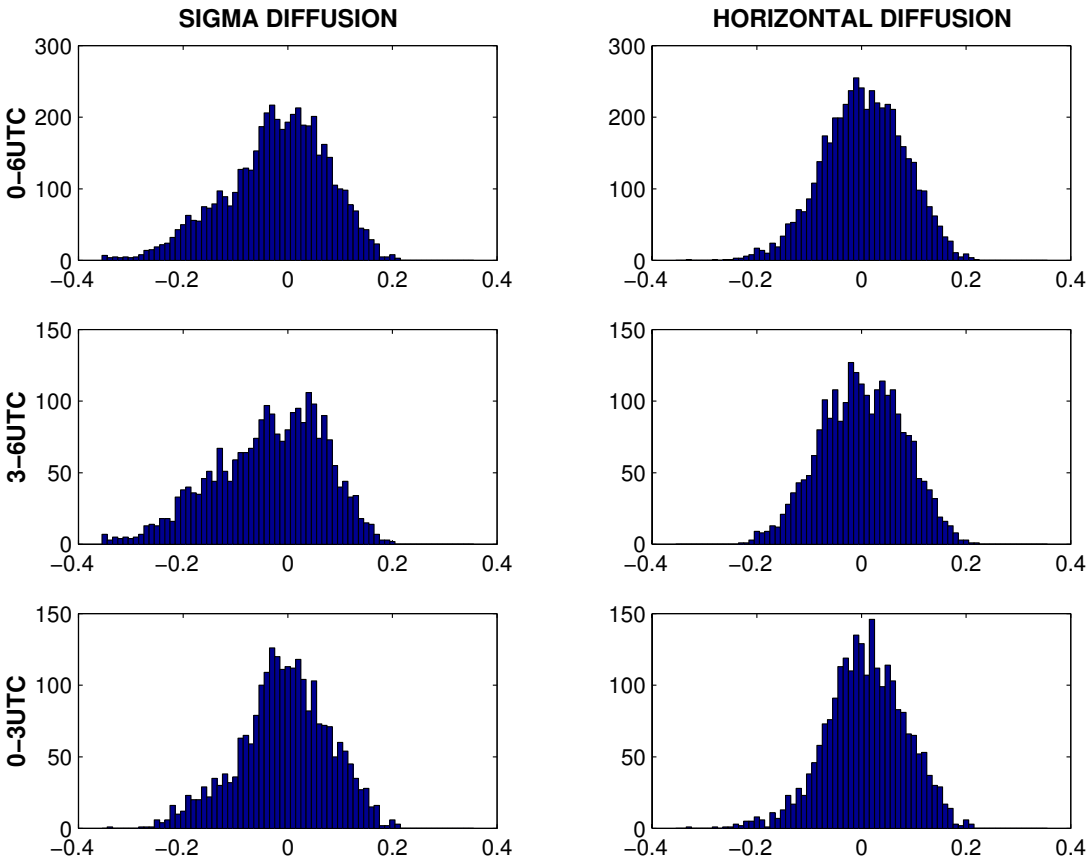

Figure 4: Frequency histogram of the relative departure of the slant wet delay. Sigma diffusion (left) vers. modified horizontal diffusion (right). The different panels show the different time intervals of the model integration. The overall statistics (0–6 UTC on August 14, 2007) is shown in the upper most panel.

to cool valleys and to heat mountains. The second option tries to establish a vertical temperature gradient within valleys leading to warmer valleys as compared to the first option. The second option effectively suppresses the erroneous temperature tendency introduced by the first option. However, both options have deficiencies (ZÄNGL, 2004a): Above mountainous terrain, a strange and noisy pattern appears in the temperature that is reminiscent of breaking gravity waves. This can be explained by the fact that diffusion along sigma surfaces induces horizontal temperature gradients over mountainous topography. As a result, pressure gradients occur and gravity waves are excited. Since gravity waves are acceptable solutions of a 4DVAR system, the minimization may try to fit the observations to these waves reducing the overall performance of 4DVAR. In both options, diffusion is computed along sigma levels for water vapor. Therefore, in both options, a spurious moisture tendency exists.

To prevent spurious temperature or moisture tendencies, diffusion should be computed truly horizontally as suggested by ZÄNGL (2002). At high elevations, this is easily done by simply interpolating between vertical coordinate surfaces. At lower model levels, truly horizontal computation may be impossible without intersecting the ground. Solutions are either to switch back to diffusion along sigma surfaces, using one-sided truly horizontal diffusion or to apply the full coordinate transformation to the horizontal diffusion operator. From an analytical point of view, the latter method is superior to vertical interpolation but it is computationally very expensive. So far we implemented the first option. Note that in narrow valleys, this option may retain some errors. The vertical interpolation is performed linearly with height for the temperature and an exponential interpolation is used for the water-vapor mixing ratio. The interpolation/extrapolation is limited to the height of the underlying model topography to avoid extreme values in complex terrain. This modified horizontal diffusion scheme and its adjoint were implemented in the MM5 4DVAR system. A brief description of the non-linear model (NLM), the tangent linear model (TLM), and the adjoint model (ADJ) is given in the Appendix.

Two model simulations were performed. The first simulation used horizontal diffusion for temperature and water vapor along terrain-following sigma-coordinates (sigma diffusion) and the second simulation applied the previously described modified horizontal diffusion

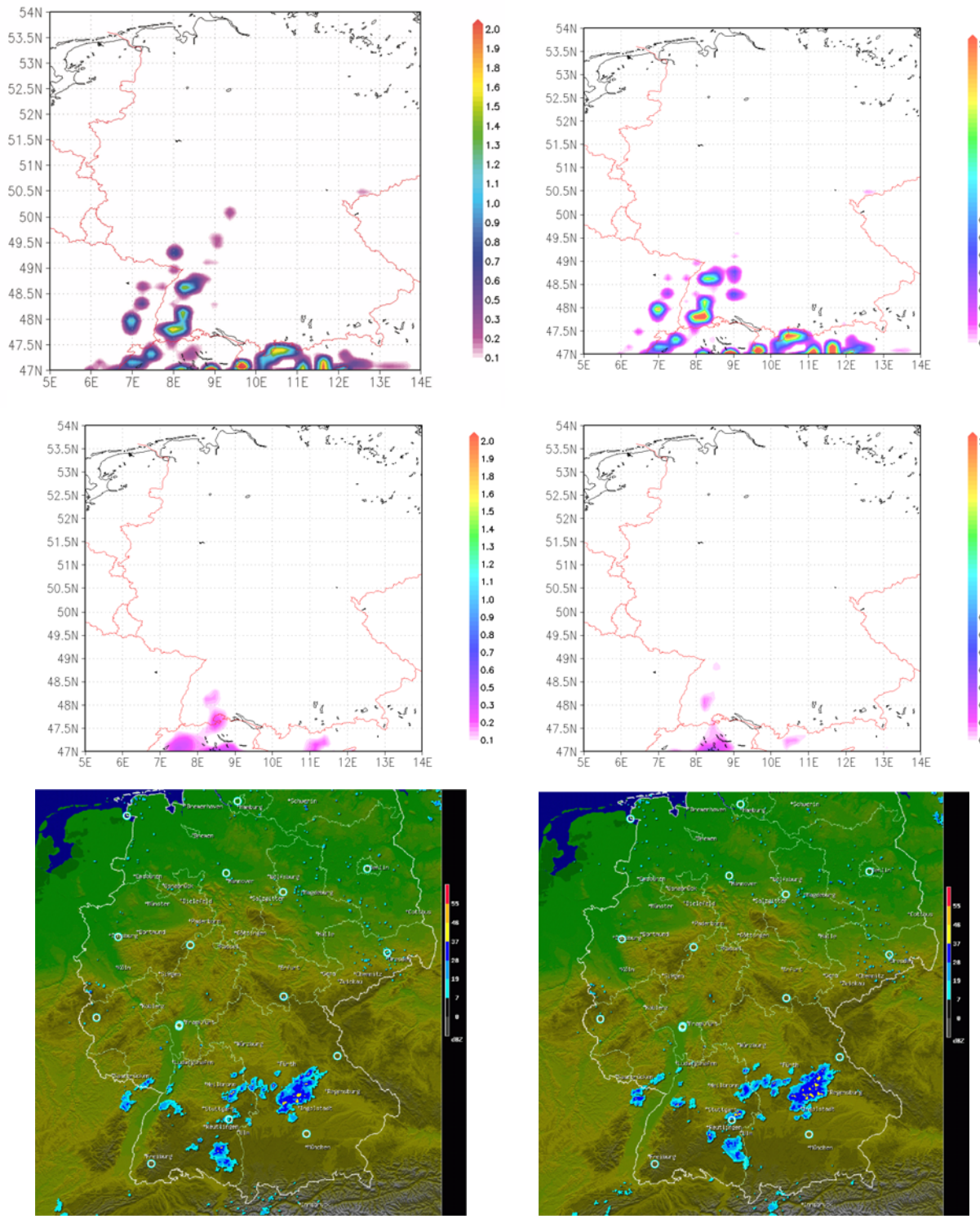

Figure 5: 15 minutes accumulated precipitation [mm] for different model physics compared qualitatively with the reflectivity of the radar composite of DWD at 00:30 UTC (left panel) and at 01:0 0UTC (right panel) on August 14, 2007. Sigma diffusion (upper panel), modified horizontal diffusion (middle panel) and radar image (lower panel).

scheme. In Figure 3, the model minus observation departures are shown as a function of the time and the elevation angle. Right from the beginning, the model simulation using sigma diffusion produces a systematic offset in time. This is not the case for the model simulation using modified horizontal diffusion. The difference between the two simulations is clearly visible in the model-minus-observation departures as a function of the elevation angle. The simulation with modified horizontal diffusion has nearly no systematic offset at high elevation

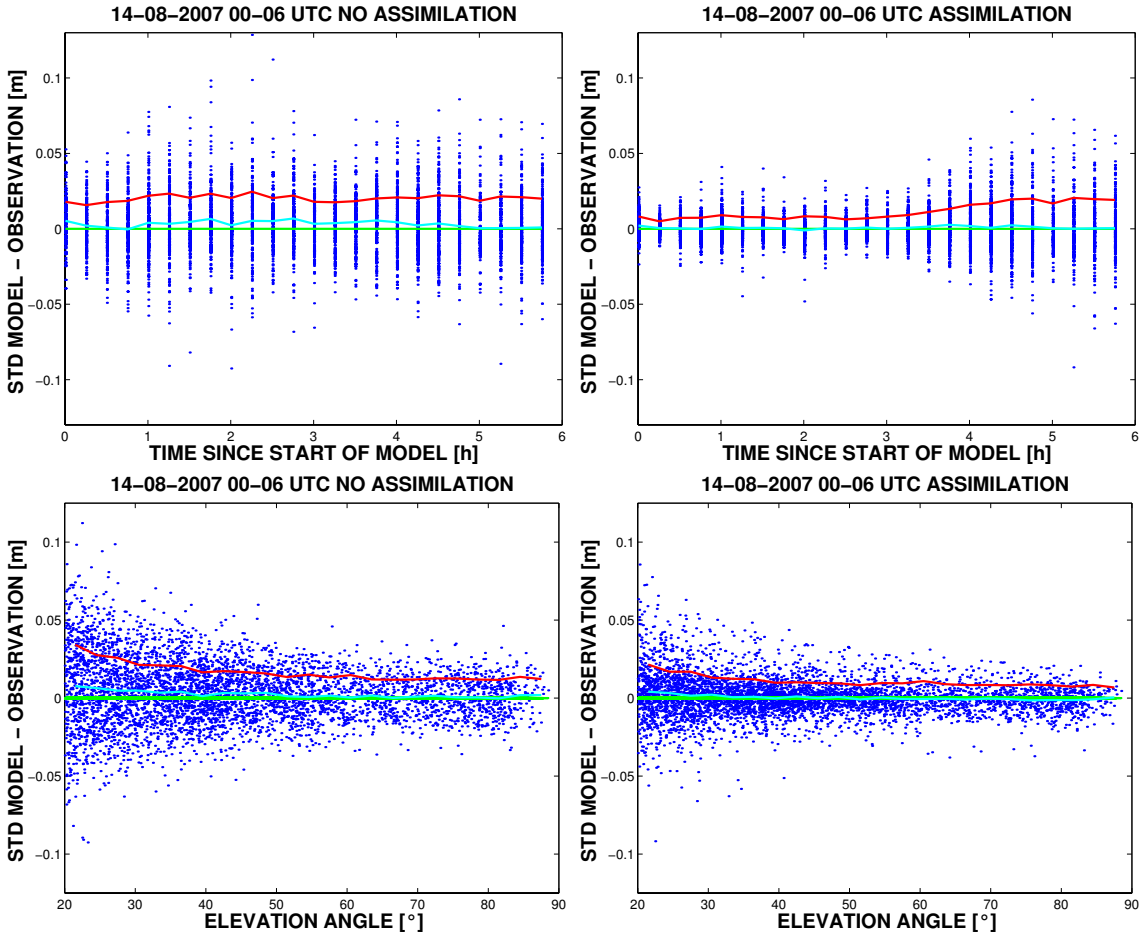

Figure 6: GPS network red: STD model minus observation departure as a function of time (top) and as a function of the elevation angle (bottom). No assimilation (left) vers. assimilation (right). The red line indicates the rmse and the cyan line the bias. The green line indicates null bias.

angles and a slighty positive bias at low elevation angles. In contrary, the simulation using sigma diffusion shows a significant negative bias at all elevation angles.

In Figure 4, a frequency histogram containing the number of STD data as a function of the relative departure of the slant wet delay is shown. The systematic model error introduced by sigma diffusion becomes obvious: The distribution of model minus observation departure is far from being a Gaussian distribution. Instantly, a shoulder separation can be observed with the simulation using sigma diffusion. Note that not at each GPS receiver a systematic error in the STD model data is produced. Comparison of STD data evaluated at GPS receivers located in mountainous terrain shows a systematic tendency. In fact, there is no difference between sigma diffusion and the modified horizontal diffusion in flat terrain.

3.2 Deep convection

Another issue in the application of MM5 4DVAR in mountainous terrain is related to the use of the Kuo convective scheme. It is known that the Kuo cumulus scheme tends to produce much convective rainfall and less resolved-scale precipitation (see e.g. GRELL et al., 1995). In addition, the convective rainfall is enhanced when horizontal diffusion is calculated along terrain-following sigma-coordinates. This can be explained by the fact that sigma diffusion transports moist (warm) air in the upper atmosphere triggering and/or enhancing convection. Thus, a precipitation forecast in mountainous terrain using the Kuo convection scheme in conjunction with sigma diffusion is doubly penalized. Figure 5 shows the 15 minutes accumulated precipitation with sigma/modified horizontal diffusion compared qualitatively to the radar composite of the DWD (Deutscher Wetterdienst). Right from the beginning of the model simulation, sigma diffusion strongly overpredicts the precipitation in mountainous terrain, namly in the Black Forest, the Vosges mountains, and the Alpine region. Precipitation instantly occurs in the model simulation using sigma diffusion in conjunction with the Kuo cumulus convective scheme. This is obviously not the case for the model simulation using the modified horizontal diffusion. The precipitation in mountainous terrain is strongly suppressed. Note that the tendency present in

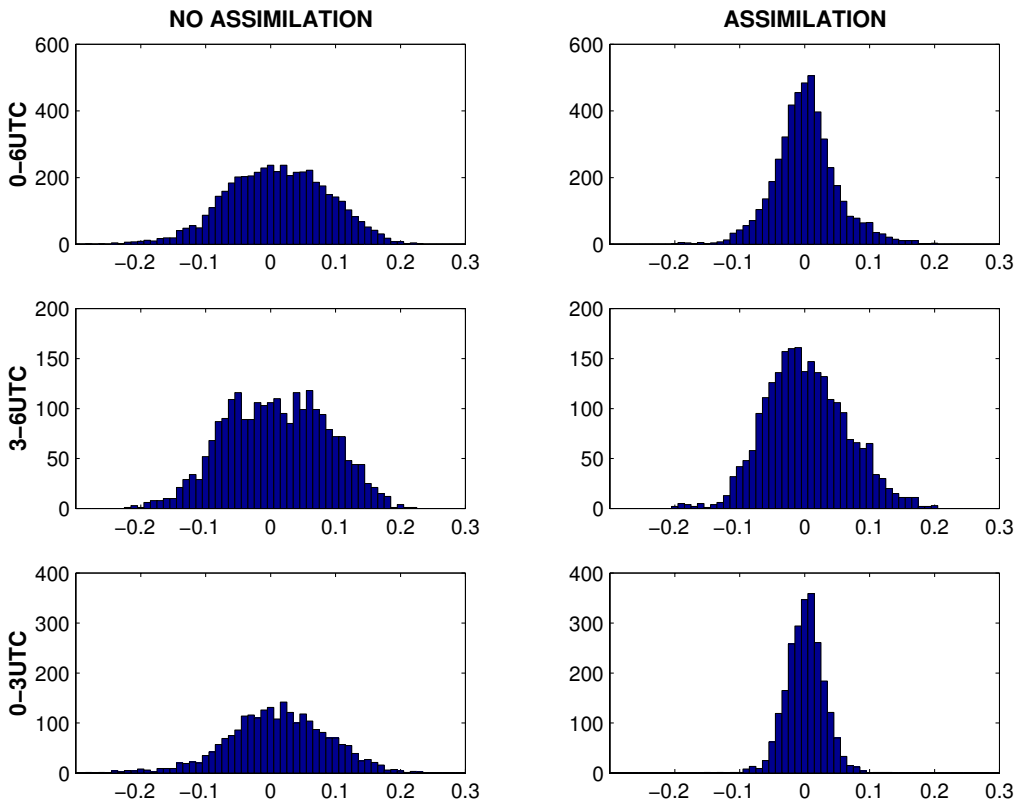

Figure 7: The different panels show the different time intervals of the model integration. The overall statistics (0–6 UTC on August 14, 2007) is shown in the upper most panel.

the model-minus-observation statistics of the STD data is strongly correlated with the over prediction of precipitation.

To bypass the tendency introduced by the Kuo cumulus scheme, we implemented the more sophisticated Grell cumulus scheme (GRELL, 1993) and its adjoint into the the MM5 4DVAR system. The forward and adjoint model of the Grell cumulus scheme already existed in an advanced version of the serial 4DVAR based on MM5 version 2 (ZOU et al., 1997), so that only minor changes were neccessary to include it in the parallel 4DVAR based on MM5v3. A first assimilation experiment is presented in the following section.

3.3 Assimilation experiment

The model configuration used in this assimilation study is given in Table 1. In the assimilation experiment, we used both updates to the MM5 4DVAR system, namely the Grell cumulus scheme and the modified horizontal diffusion scheme. The result of the assimilation experiment B is discussed briefly at the end of this section.

The assimilation frequency was 30 minutes and each STD of the used GPS receivers enters the assimilation system. The assimilation window was 3 hours. For validation purpose, we set up two networks, network red and network green. An overview of the geographical location is presented in Figure 2. Both networks consist of around 30 GPS receivers distributed over Europe, simultaneously tracking several satellites with different azimuth and elevation angels. The membership of a specific GPS receiver to one of the networks is more or less randomly chosen, except for the upwind stations in the westernmost part that were included in the red network. The network red provides STD data for the assimilation. In contrast, the network green is the observing network, meaning that STD data provided by this network is not assimilated. Since it is of interest whether independent upper air measurements support the results gained by the STD data assimilation, radiosondes are used for intercomparison. The chosen day for this experiment is the same as in the previous case. Meteosat satellite data shows that the area of interest (south Germany) was affected by clouds, a situation where we expect to benefit from the assimilation of GPS STD data.

The following questions regarding STD 4DVAR are adressed: 1) Does the STD 4DVAR algorithm work properly? 2) Is there a detectable and significant impact of the STD data in the assimilation window as well as after the assimilation window? 3) Is there any indication that the humidity field is better represented with assimilation than without assimilation? Is the improvement in the humidity field significant? 4) Is it possible to easily validate the results with independent upper air measure-

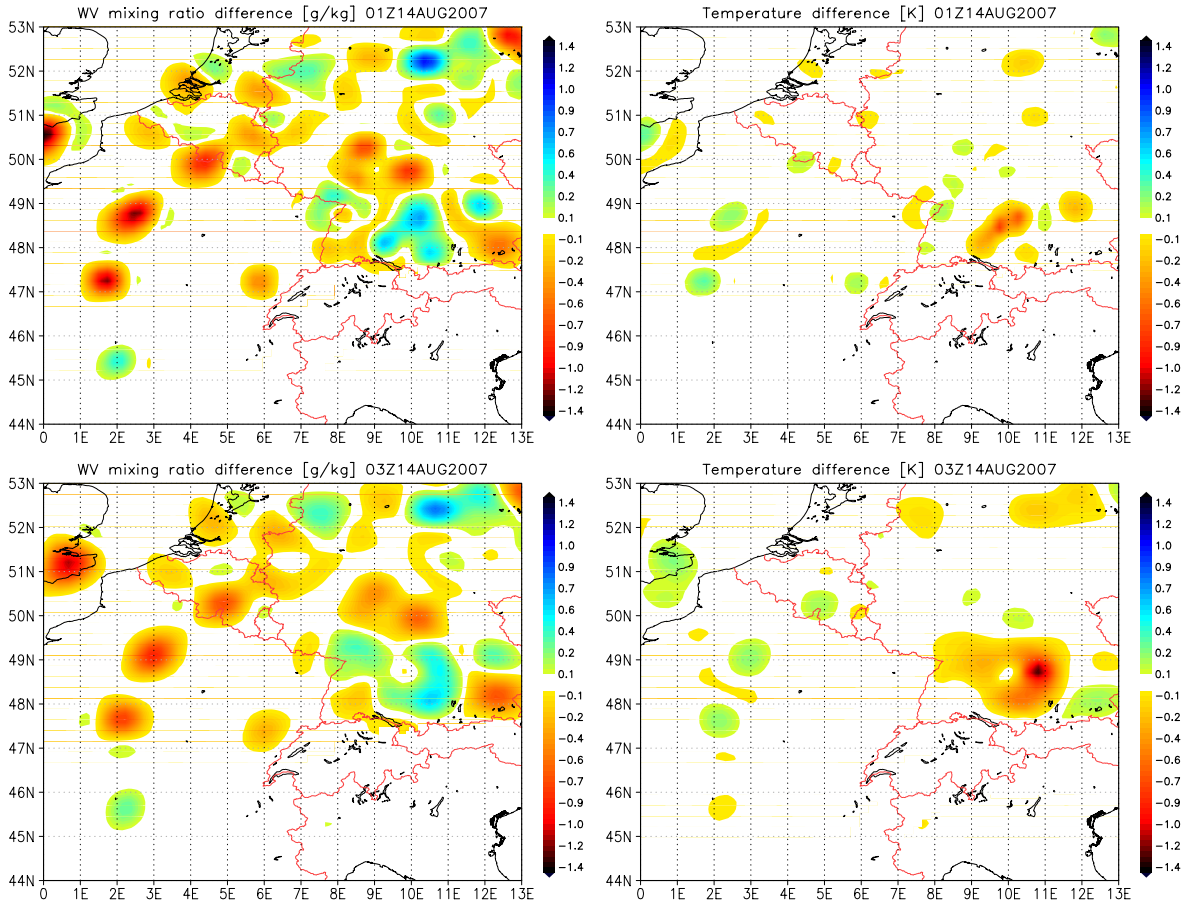

Figure 8: Difference between assimilation and no assimilation in water-vapor mixing ratio [g/kg] (left) and temperature [K] (right) in 850 hPa at 1 UTC (upper panel) and 3 UTC (lower panel) valid on August 14, 2007.

ments? 5) Can we expect that the STD 4DVAR has a positive impact on QPF?

In connection with question 1, it is important to note that the 4DVAR works properly from a technical point of view. The modified TLM and ADJ routines are tested for correctness using the standart comparison of the TLM and finite difference-derived NLM gradients to check correctness of the TLM and the definition of the adjoint to check for consistency of the TLM and the ADJ. For details on the nature of those tests see ZOU et al. (1997). The minimization (convergence) of the cost function in 4DVAR worked properly.

To answer the second question, we took a look at the statistics of the red network, which is illustrated in Figure 6. The small bias appearing in the control run is reduced to zero and the rmse is significantly reduced in the assimilation window as well as after the assimilation window. However the impact seems to fade away quickly. This is due to the fact that air masses are advected above GPS receivers with the ambient wind direction from the west. Note that the frequency of assimilation is 30 minutes only but 15 minutes data are evaluated. A frequency histogram of the relative departure of the slant wet delays is shown in Figure 7. It is obvious that the assimilation of STD data has a detectable and significant impact in the assimilation window as well as after the assimilation window. The difference in the water vapor field in 850 hPa between assimilation and no assimilation reaches values up to 1 g/kg, the difference in the temperature reaches 1 K and in the wind field 1 m/s. Figure 8 shows the difference between the simulation with and without assimilation in the water vapor field and the temperature.

To answer the third question, we take a look at the green network. Figure 9 indicates that the humidity content is better represented with assimilation. The rmse is reduced during the six hours of the model integration. If we take a look at Figure 10 showing the frequency histogram of the relative departure of the slant wet delay of the green network, a tendency pointing to the right direction is obvious. Figure 10 indicates that the STD data of the green network support the results gained by the assimilation of the STD data of the red network. At this point, the following important conclusion can be drawn: If we in trust the accuracy of model physics as well as in the accuracy of the observations, the assimilation improves the representation of the humidity content.

For intercomparison with independent upper air field measurements, we evaluated all radiosondes from central Europe between 0 UTC and 6 UTC which were

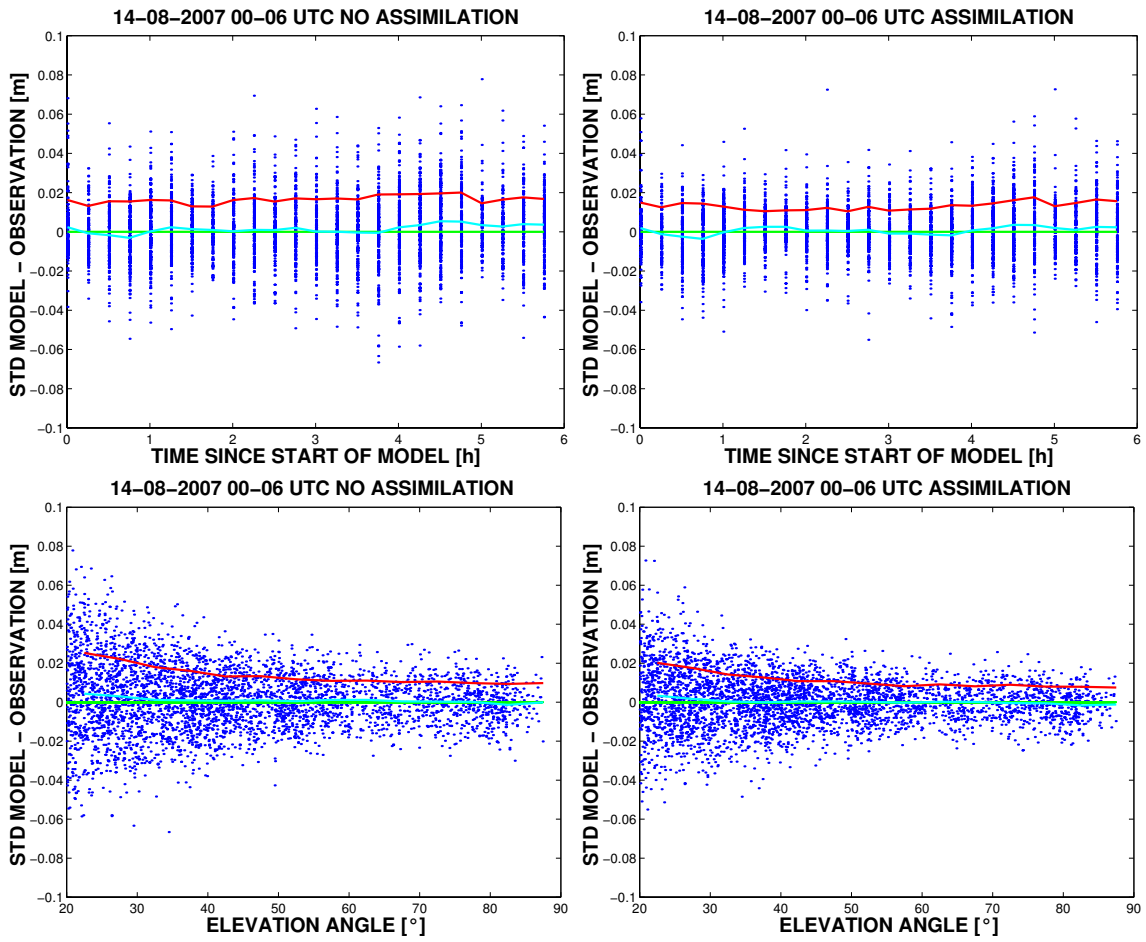

Figure 9: GPS network green: STD model minus observation departure as a function of time (top) and as a function of the elevation angle (bottom). No assimilation (left) vers. assimilation (right). The red line indicates the rmse and the cyan line the bias. The green line indicates null bias.

available from the ECMWF MARS archive. Numerous radiosondes are as far away from the impact region as some of the GPS receivers in the green network. For those radiosondes we do not observe any difference between the assimilation and the control run. Most of the radiosondes are launched at 0 UTC and some at 6 UTC. Regarding those profiles where we see an impact, we observe that the structure, which is present in the radiosonde measurement but not in the control run, is partly generated by the assimilation. However, there are radiosondes and/or specific locations where the water vapor content seems to be better represented in the control run compared to the assimilation run. An example of a radiosonde launched in the region of interest (southwest Germany) is given in Figure 11. At this radiosonde location, the assimilation enhanced the water-vapor content in the lower troposphere. The simulation with assimilation is in better agreement with the radiosonde compared to the simulation without assimilation except at one height level in the lower troposphere. But at this location we observe another interesting feature: A small kink in the water vapor profile is introduced by the assimilation, which is also present in the radiosonde measurement, but not in the simulation without assimilation. We attribute this to the ability of the 4DVAR to self-generate physically consistent structure functions during model integration, provided that the model physics is accurate enough and the background errors are reasonable. In any case, due to the sparse character of water-vapor observations, it is difficult to draw a significant conclusion regarding the validation with independent upper air field measurements, at least for a short-range forecast.

To gain some insight into the precipitation predicted by the simulations with and without assimilation of STD data, Figure 12 shows the 15 minutes accumulated precipitation qualitatively compared to the radar composite of the DWD. We observe that both simulations do not show any precipitation in the Black Forest, in the Vosges mountains, or in the Alpine region. The situation is very different from the previous simulations using the Kuo cumulus convection scheme. The simulation with assimilation predicts the initiation of convection very close to the region where it was observed. Similar to the radar image, the convective system moves with the ambient flow from southwest to northeast before it vanishes in the simulation. A close inspection in the area of interest

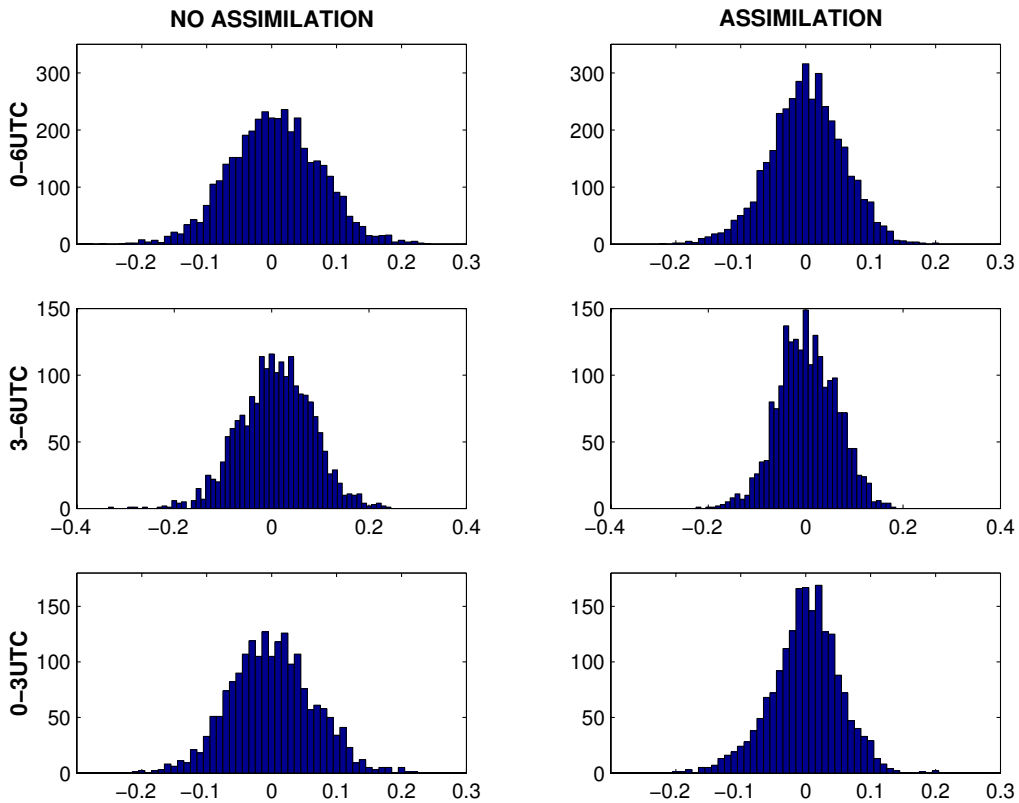

Figure 10: GPS network green: Frequency histogram of the relative departure of the slant wet delay. The different panels show the different time intervals of the model integration. The overall statistics (0–6 UTC on August 14, 2007) is shown in the upper most panel.

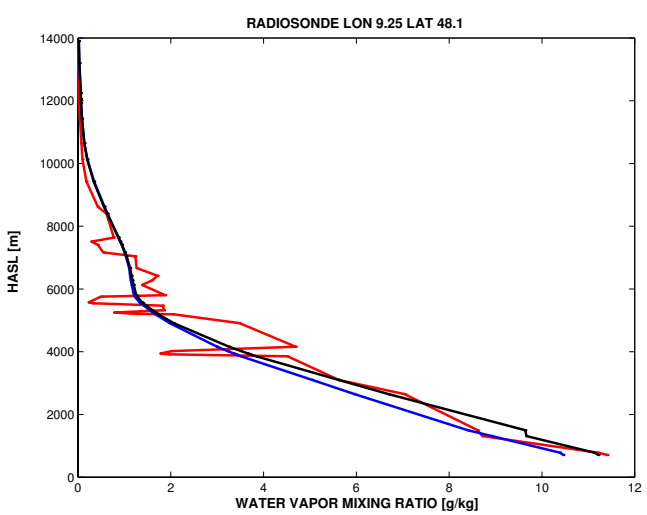

Figure 11: Radiosonde profile close to Stuttgart, Germany at 1 UTC on August 14, 2007 (WMO ID 10739). The red line indicates the radiosonde measurement, the blue line indicates the model prediction without assimilation and the black line indicates the model prediction with assimilation of the STD data.

indicates that the local enhancement of water vapor in the lower troposphere of the order of 1 g/kg (see Fig. 8) due to the assimilation of the GPS data is the primary source that permits to simulate the observed convective system.

Finally we study the result of the assimilation experiment B. The following question shall be answered: What is the impact on the model-minus-observation statistics, if the Kuo cumulus scheme in conjunction with sigma diffusion is used in 4DVAR and a model forecast with more sophisticated physics, i.e. the Grell cumulus scheme in conjunction with the modified horizontal diffusion scheme, is performed? The result of this simulation is illustrated in Figure 13. Although the rmse is reduced, a significant bias is introduced. The analysis gained by 4DVAR using simplified physics is not optimal. The 4DVAR compensates the lack of water vapor arising due to the erroneous moisture and temperature tendency introduced by the poor model physics (see left panel of Figure 4). Since this erroneous tendency is absent using more sophisticated physics, in the free model forecast a positive bias of the order of magnitude shown in the left image of Figure 4 appears. The initial state generated by the 4DVAR with simplified physics leads to an erroneous result.

4 Conclusion

This article describes the development of tools for routine data assimilation of real STD observations with the

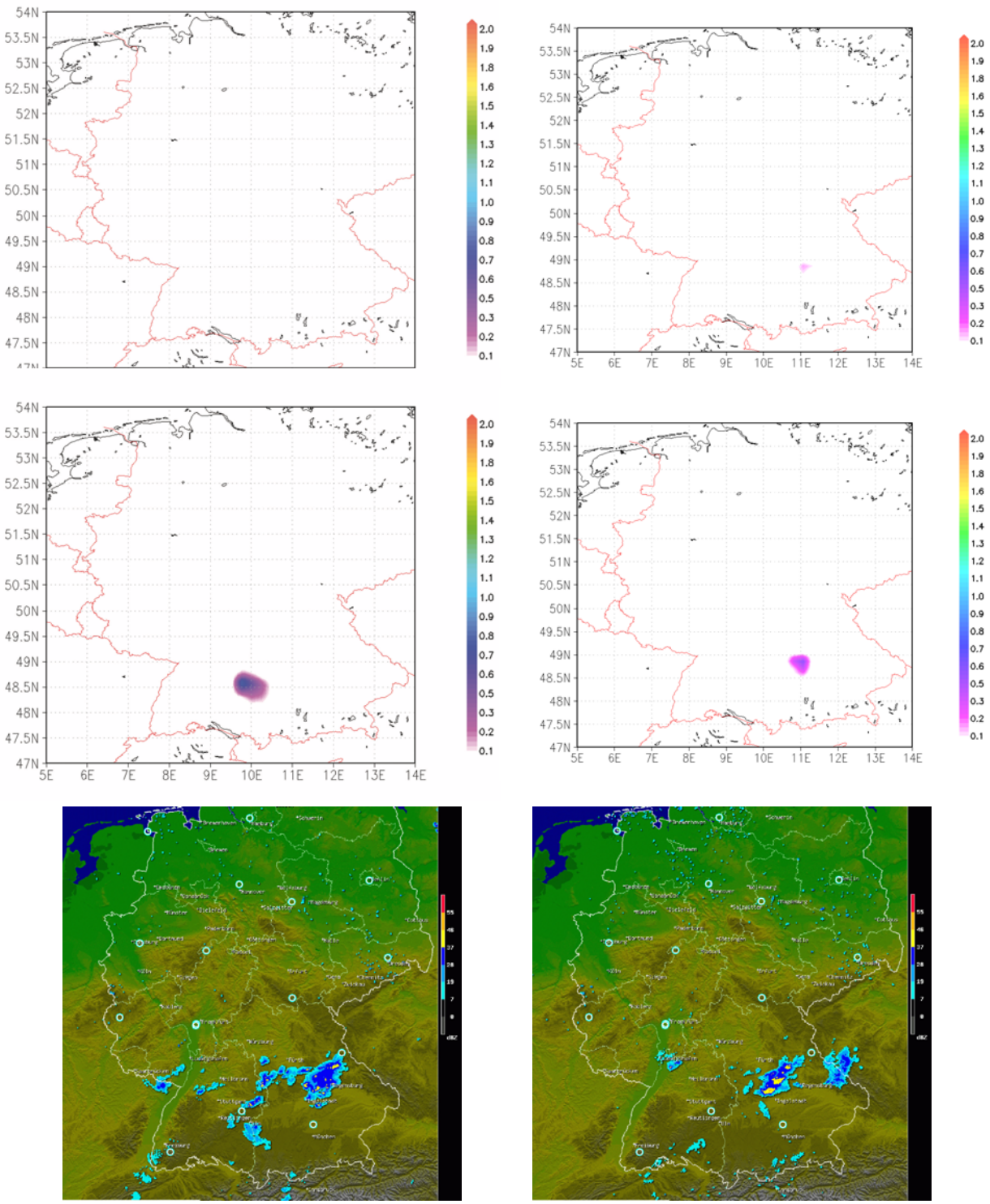

Figure 12: 15 min accumulated precipitation [mm] with and without assimilation compared qualitatively with the reflectivity of the radar composite of DWD at 01:30 UTC (left panel) and at 04:00 UTC (right panel) on August 14, 2007. No assimilation (upper panel), assimilation (middle panel) and radar image (lower panel).

MM5 modeling system. The STD forward operator was introduced, which allowed model validation and the assimilation of STD data in the MPI environment of the MM5 4DVAR system.

A model experiment was conducted, which demonstrates the necessity of accurate model physics in the variational assimilation system. The convection scheme and the implementation of horizontal diffusion turn out to be key components regarding the assimilation of high-

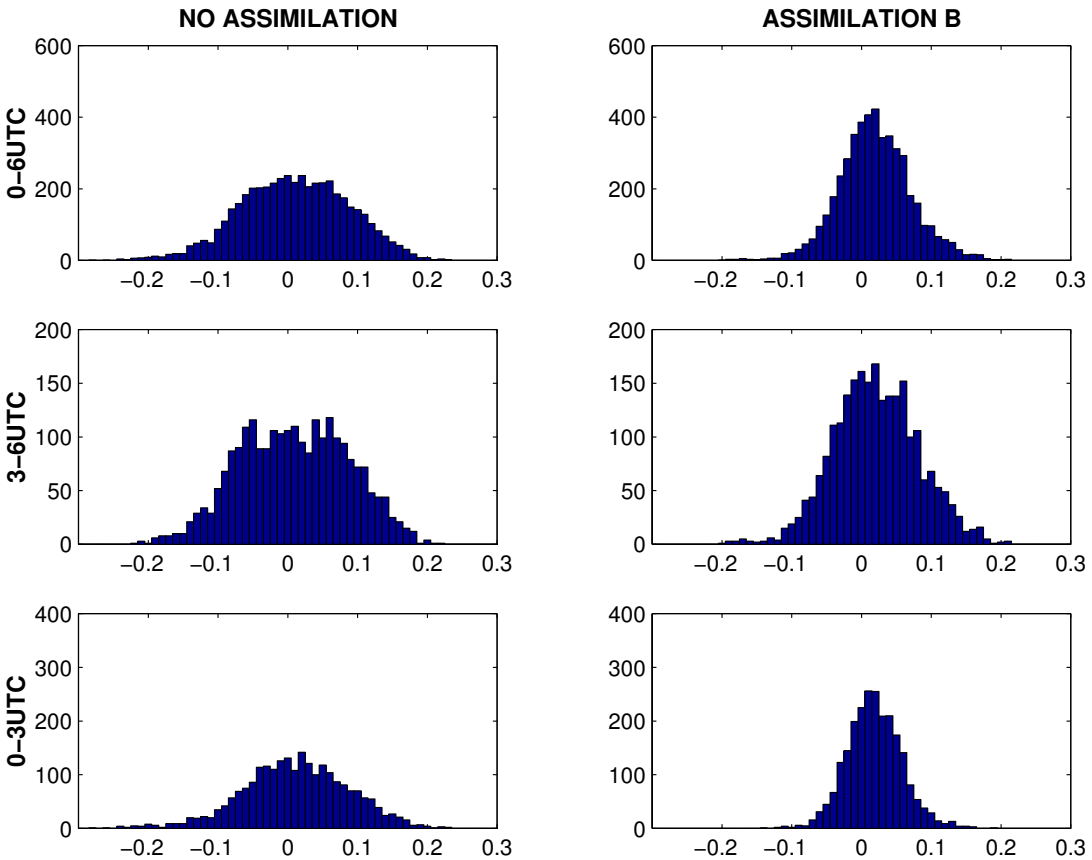

Figure 13: GPS network red: Frequency histogram of the relative departure of the slant wet delay. The different panels show the different time intervals of the model integration. The overall statistics (0–6 UTC on August 14, 2007) is shown in the upper most panel. The assimilation is performed using the Kuo cumulus scheme in conjunction with sigma diffusion. The model forecast is performed using the Grell cumulus scheme and the modified horizontal diffusion.

resolution observations related to water vapor such as STD data. It is important to note that the particular day chosen for this experiment is not an exceptional day. Rather, this particular day was chosen in order to highlight the erroneous behaviour in mountainous terrain of the former model physics incorporated in the MM5 4DVAR.

A set of modifications to the existing MM5 4DVAR system was introduced. For the temperature and the water-vapor mixing ratio a vertical interpolation is applied to compute a truly horizontal diffusion at those grid points where such a calculation is possible. Close to the ground, the horizontal diffusion is computed along the coordinate surfaces. The improved scheme for computing diffusion was validated using high-temporal resolution STD data. Furthermore, the Grell cumulus scheme was implemented in the forward model as well as in the adjoint part of the 4DVAR system in order to eliminate the observed tendency (overprediction of precipitation) introduced by the Kuo cumulus convective scheme. Although we cannot preclude any other remaining deficiencies in model physics, we believe this was the most important systematic model error.

Regarding the use of ground-based GPS data for model evaluation, the following conclusion can be drawn: A spurious tendency present in the model minus observation statistics of the STD data is strongly related to the misplacement and/or the enhancement/suppression of precipitation.

Finally an assimilation experiment with the improved MM5 4DVAR system was presented. The results are promising and show that:

1) the 4DVAR of STD data is highly effective in reducing the model minus observation departure, 2) the impact is area wide, reasonable and significant, 3) STD data of an independent network of GPS receivers confirm the results gained by 4DVAR, 4) in a convective active region, radiosonde measurements confirm the results gained by 4DVAR, 5) a qualitative comparison with radar data shows that the 4DVAR of STD data improves the simulation of an observed convective system and 6) the use of simplified physics in the MM5 4DVAR (the Kuo cumulus scheme in conjunction with sigma diffusion) leads to an erroneous analysis.

Since the forward model in this study does not take into account the ray bending at low elevation angles, the

STD data used for validation and assimilation are restricted to elevation angles above 20 degree at the GPS receiver. In the future, we plan to account for the bending so that we can take full advantage of the STD data at low elevation angles. Recently a 3D-raytracing algorithm based on the idea of PETROV (2008) was developed. The tangent linear and adjoint code sucessfully passed first tests. The results indicate that the assimilation of STD data down to about 7 degrees is feasible. Therefore the sensitive region will be increased considerably.

The tuning of background/observation errors as well as the development of a more sophisticated data selection algorithm are subject to future research. Comprehensive studies on a statistical significant basis are in preparation in connection with the WWRP projects COPS (WULFMEYER et al., 2008) and MAP D-PHASE (ROTACH et al., submitted).

Appendix

A brief description of the modified horizontal diffusion scheme (NLM, TLM and ADJ) is given. We focus on the approximation of the fourth partial derivative of water vapor in the MM5 terrain following coordinate system. The approximation of the fourth partial derivative of temperature is treated in a similar manner except that the reconstruction of model variables is linear. For readers which are not familiar with adjoint code construction see ZOU et al. (1997).

Let I, J and K denote the grid point indices of a point in model space (with coordinates y, x and z) at which the fourth partial derivative of water vapor Ω with respect to the y direction is computed. The second-order accurate discretization of the fourth partial derivative is altered to be:

$$\begin{aligned}&\Omega_{IJK} = \\ &\big[\ 1\cdot Q_{I+2JA}(Q_{I+2JA}/Q_{I+2JA-1})^{LA} \\ &-4\cdot Q_{I+1JB}(Q_{I+1JB}/Q_{I+1JB-1})^{LB} \\ &-4\cdot Q_{I-1JC}(Q_{I-1JC}/Q_{I-1JC-1})^{LC} \\ &+1\cdot Q_{I-2JD}(Q_{I-2JD}/Q_{I-2JD-1})^{LD} \\ &+6\cdot Q_{IJK}\big]/\Delta y^4\end{aligned} \tag{0.1}$$

where Q denotes the gridded water-vapor field and Δy denotes the grid increment in y direction. The relevant reconstruction coefficients are computed as follows:

$$\begin{aligned}CA &= max(H_{IJK}, S_{I+2J}-\beta_{I+2J}) \\ CB &= max(H_{IJK}, S_{I+1J}-\beta_{I+1J}) \\ CC &= max(H_{IJK}, S_{I-1J}-\beta_{I-1J}) \\ CD &= max(H_{IJK}, S_{I-2J}-\beta_{I-2J}) \\ LA &= (CA-H_{I+2JA})/(H_{I+2JA}-H_{I+2JA-1}) \\ LB &= (CB-H_{I+1JB})/(H_{I+1JB}-H_{I+1JB-1}) \\ LC &= (CC-H_{I-1JC})/(H_{I-1JC}-H_{I-1JC-1}) \\ LD &= (CD-H_{I-2JD})/(H_{I-2JD}-H_{I-2JD-1})\end{aligned} \tag{0.2}$$

where H stores grid point heights and S stores the heights of the underlying model topography. The integers A, B, C and D denote the grid point indices in the z direction of adjacent grid points. The threshold $\beta \geq 0$ limits the reconstruction below the model topography. If $LA = LB = LC = LD = 0$ and $A = B = C = D = K$ the expression for sigma diffusion is recovered, i.e. there is no difference between sigma diffusion and the modified horizontal diffusion scheme in flat terrain. To date, we do not allow the reconstruction of variables below the model topography ($\beta = 0$) since it is not clear to what extend the extrapolation can be regarded as representative. A dependency of β on the local gradient seems to be resonable. The tuning of β is the subject of future research. The computation of the TLM section from the NLM section leads to:

$$\begin{aligned}&\delta\Omega_{IJK} = \\ &\big[\ 1\cdot(LA+1)\delta Q_{I+2JA}(Q_{I+2JA}/Q_{I+2JA-1})^{LA} \\ &-4\cdot(LB+1)\delta Q_{I+1JB}(Q_{I+1JB}/Q_{I+1JB-1})^{LB} \\ &-4\cdot(LC+1)\delta Q_{I-1JC}(Q_{I-1JC}/Q_{I-1JC-1})^{LC} \\ &+1\cdot(LD+1)\delta Q_{I-2JD}(Q_{I-2JD}/Q_{I-2JD-1})^{LD} \\ &-1\cdot LA\delta Q_{I+2JA-1}(Q_{I+2JA}/Q_{I+2JA-1})^{LA+1} \\ &+4\cdot LB\delta Q_{I+1JB-1}(Q_{I+1JB}/Q_{I+1JB-1})^{LB+1} \\ &+4\cdot LC\delta Q_{I-1JC-1}(Q_{I-1JC}/Q_{I-1JC-1})^{LC+1} \\ &-1\cdot LD\delta Q_{I-2JD-1}(Q_{I-2JD}/Q_{I-2JD-1})^{LD+1} \\ &+6\cdot\delta Q_{IJK}\big]/\Delta y^4\end{aligned} \tag{0.3}$$

where δQ denotes the gridded water vapor increments and the increment of the fourth partial derivative of water vapor with respect to the y direction is denoted as $\delta\Omega$. Note that the reconstruction coefficients are passive variables since grid point heights are constants (the 4DVAR is based on the non-hydrostatic version of the MM5) and the threshold β is not related to any active variable. If $\delta\hat{Q}$ and $\delta\hat{\Omega}$ denote the adjoint variables, the corresponding

ADJ model section reads as:

$$\begin{aligned}
\delta\hat{Q}_{I+2JA} &= \delta\hat{Q}_{I+2JA} + 1\cdot(LA+1)/\Delta y^4 \quad (0.4)\\
&\quad \cdot(Q_{I+2JA}/Q_{I+2JA-1})^{LA}\delta\hat{\Omega}_{IJK}\\
\delta\hat{Q}_{I+1JB} &= \delta\hat{Q}_{I+1JB} - 4\cdot(LB+1)/\Delta y^4\\
&\quad \cdot(Q_{I+1JB}/Q_{I+1JB-1})^{LB}\delta\hat{\Omega}_{IJK}\\
\delta\hat{Q}_{I-1JC} &= \delta\hat{Q}_{I-1JC} - 4\cdot(LC+1)/\Delta y^4\\
&\quad \cdot(Q_{I-1JC}/Q_{I-1JC-1})^{LC}\delta\hat{\Omega}_{IJK}\\
\delta\hat{Q}_{I-2JD} &= \delta\hat{Q}_{I-2JD} + 1\cdot(LD+1)/\Delta y^4\\
&\quad \cdot(Q_{I-2JD}/Q_{I-2JD-1})^{LD}\delta\hat{\Omega}_{IJK}\\
\delta\hat{Q}_{I+2JA-1} &= \delta\hat{Q}_{I+2JA-1} - 1\cdot LA/\Delta y^4\\
&\quad \cdot(Q_{I+2JA}/Q_{I+2JA-1})^{LA+1}\delta\hat{\Omega}_{IJK}\\
\delta\hat{Q}_{I+1JB-1} &= \delta\hat{Q}_{I+1JB-1} + 4\cdot LB/\Delta y^4\\
&\quad \cdot(Q_{I+1JB}/Q_{I+1JB-1})^{LB+1}\delta\hat{\Omega}_{IJK}\\
\delta\hat{Q}_{I-1JC-1} &= \delta\hat{Q}_{I-1JC-1} + 4\cdot LC/\Delta y^4\\
&\quad \cdot(Q_{I-1JC}/Q_{I-1JC-1})^{LC+1}\delta\hat{\Omega}_{IJK}\\
\delta\hat{Q}_{I-2JD-1} &= \delta\hat{Q}_{I-2JD-1} - 1\cdot LD/\Delta y^4\\
&\quad \cdot(Q_{I-2JD}/Q_{I-2JD-1})^{LD+1}\delta\hat{\Omega}_{IJK}\\
\delta\hat{Q}_{IJK} &= \delta\hat{Q}_{IJK} + 6\cdot/\Delta y^4\delta\hat{\Omega}_{IJK}\\
\delta\hat{\Omega}_{IJK} &= 0
\end{aligned}$$

The same procedure is applied in the x direction. Once the fourth partial derivative of water vapor with respect to y and x is computed, the update of the water vapor tendency due to horizontal diffusion is straightforward. Note however, that the diffusion coefficient K_h in Equation 3.1 must be treated as an active variable since it is a function of the local deformation of the wind field (see GRELL et al., 1995 for further details on K_h).

Acknowledgments

We appreciate the access to the ECMWF analysis and the radar data provided by DWD. The author wants to thank T. SCHWITALLA for helpful tips regarding the graphics.

References

ABRAMOWITZ, M., I.A. STEGUN, 1972: Handbook of Mathematical Functions with Formulas, Graphs and Mathematical Tables, 9th printing. – Dover, New York.

BEHRENDT, A., T. NAKAMURA, M. ONISHI, R. BAUMGART, T. TSUDA, 2002: Combined Raman lidar for the measurement of atmospheric temperature, water vapor, particle extiction coefficient, and particle backscatter coefficient. – Appl. Opt. **36**, 7657–7666.

BEVIS, M., S. BUSINGER, T. HERRING, C. ROCKEN, R. ANTHES, R. WARE, 1992: GPS meteorology: Remote sensing of atmospheric water vapor using the Global Positioning System. – J. Geophys. Res. **97**, 15787–15801.

BOSSER, P., O. BOCK, J. PELON, C. THOM, 2007: An improved mean-gravity model for GPS hydrostatic delay calibration. – Geosci. Remote Sens. Lett. **4**, 3–7.

BOUTTIER, F., P. COURTIER, 1999: Data assimilation concepts and methods. Technical report, Meteorological Training Course Lecture Series, ECMWF, European Center for Medium Range Weather Forecasting, Reading, UK available online on: www.ecmwf.int/newsevents/training/rcoursenotes/DATAASSIMILATION/index.html.

CUCURULL, L., B. NAVASCUES, G. RUFFINI, P. ELÓSEGUI, A. RIUS, J. VILÁ, 2000: The use of GPS to validate NWP systems: The HIRLAM model. – J. Atmos. Oceanic Technol. **17**, 773–787.

DICK, G., G. GENDT, C. REIGBER, 2001: First experience with near real-time water vapor estimation in a german GPS network. – J. Atmos. Solar-Terrestrial Phys. **63**, 1295–1304.

ELGERED, G., J. DAVIS, T. HERRING, I. SHAPIRO, 1991: Geodesy by radio interferometry: Water vapor radiometry for estimation of the wet delay. – J. Geophys. Res. **96**.

ERESMAA, R., H. JÄRVINEN, 2004: A line of sight observation operator for ground-based GPS slant delays. – TOUGH project deliverable **39**, available at http://tough.dmi.dk

ERESMAA, R., H. JÄRVINEN, S. NIEMELÄ, K. SALONEN, 2007: Azimuthal asymmetry in ground-based GPS slant delay observations and their NWP model counterparts. – Atmos. Chem. Phys. Discuss. **7**, 3179–3202.

FISHER, M., 2001: Assimilation techniques: 4DVAR. Technical report, Meteorological Training Course Lecture Series, ECMWF. – European Center for Medium Range Weather Forecasting, Reading, UK, available at: www.ecmwf.int/newsevents/training/rcoursenotes/DATAASSIMILATION/index.html

GRELL, G.A., 1993: Prognostic evaluation of assumptions used by cumulus parameterizations. – Mon. Wea. Rev. **121**, 764–787.

GRELL, G., J. DUDHIA, R. STAUFFER, 1995: A description of the fith-generation Penn State/NCAR mesoscale model (MM5). – Technical Note TN-398+STR, 122 pp.

GRZESCHIK, M., H.-S. BAUER, V. WULFMEYER, D. ENGELBART, U. WANDINGER, I. MATTIS, D. ALTHAUSEN, R. ENGELMANN, M. TESCHE, A. RIEDE, 2008: Four-dimensional variational data analysis of water vapor raman lidar data and their impact on mesoscale forecasts. – J. Atmos. Oceanic Technol. **25**, 1437–1453.

GUSTAFSSON, N., 2007: Discussion on '4d-var or enkf?'. – Tellus A **59**, 774–777.

HA, S., Y.-H. KUO, Y.-R. GUO, G.-H. LIM, 2003: Variational assimilation of slant-path delay measurements from a hypothetical ground-based GPS network. Part I: Comparison with precipitable water assimilation. – Mon. Wea. Rev. **131**, 2635–2655.

HAAN, S., VAN DER H. MAREL, S. BARLAG, 2002: Comparison of GPS slant delay measurements to a numerical model: case study of a cold front passage. – Phys. Chem. Earth. **27**, 317–322.

HONG, S., H. PAN, 1996: Nonlocal boundary layer vertical diffusion in a medium-range forecast model. – Mon. Wea. Rev. **124**, 2322–2339.

JÄRVINEN, H., E. ERESMAA, H. VEDEL, S. KIRSTI, N. SAMI, J. DEVRIES, 2007: A variational data assimilation system for ground-based GPS slant delays. – Quart. J. Roy. Meteor. Soc. **133**, 969–980.

KALNAY, E., H. LI, T. MIYOSHI, S. YANG, J. BALLABRERA-POY, 2007: 4D-Var or Ensemble Kalman Filter?. – Tellus **59**, 758–773.

KUO, H.L., 1974: Further studies of the influence of cumulus convection on larger-scale flow. – J. Atmos. Sci. **31**, 1232–1240.

NEHRKORN, T., G.D. MODICA, M. CERNIGLIA, F.H. RUGGIERO, J.G. MICHALAKES, X. ZOU, 2002: 4DVAR development using an automatic code generator: Application to MM5v3. – In: Proc. 12th PSU/NCAR Mesoscale Modeling System Users Workshop, Boulder, CO, U.S.

PARRISH, D.F., J.C. DERBER, 1992: The national meteorological centre's spectral statistical-interpolation analysis system. – Mon. Wea. Rev. **120**, 1747–1763.

PETROV, L., 2008: Modeling slanted path delay using numerical 4D models of the atmosphere. – Geophys. Res. Abstracts **10**, EGU2008-A-11093, aviable at www.cosis.net/abstracts/EGU2008/11093/EGU2008-A-11093.pdf

POLI, P., P. MOLL, F. RABIER, G. DESROZIERS, B. CHAPNIK, L. BERRE, S.B. HEALY, E. ANDERSSON, F.-Z.E. GUELAI, 2007: Forecast impact studies of zenith total delay data from European near real-time GPS stations in Meteo France 4DVAR. – J. Geophys. Res. **112**, 1–16.

ROTACH, M., M. ARPAGAUS, M. DORNINGER, C. HEGG, J. FRICK, A. MONTANI, R. RANZI, F. BOUTTIER, A. BUZZI, G. FRUSTACI, K. MYLNE, E. RICHARD, A. ROSSA, C. SCHÄR, M. STAUDINGER, H. VOLKERT, V. WULFMEYER, H.-S. BAUER, F. AMENT, M. DENHARD, F. FUNDEL, U. GERMANN, M. STOLL, submitted: MAP D-PHASE: Real-time demonstration of weather forecast quality in the Alpine Region. – Bull. Amer. Meteor. Soc.

RUGGIERO, F.H., G.D. MODICA, T. NEHRKORN, M. CERNIGLIA, J. MICHALAKES, X. ZOU, 2001: Development of an MM5-based fourdimensional variational assimilation system for distributed memory multiprocessor computers. – In: Proc. HPCMP 2001 User's Group Conf., Biloxi, MS, U.S. Naval Oceanographic Office.

RUGGIERO, F., J. MICHALAKES, T. NEHRKORN, G. MODICA, M. CERNIGLIA, X. ZOU, D. NORQUIST, 2002: Performance of the scalable mesoscale four dimensional variational assimilation system. – Technical report, Department of Defense High Performance Compiting Moderization Program, UGC 2002, Austin, Texas, U.S.

SAASTAMOINEN, J., 1972: The use of artificial satellites for geodesy, Atmospheric correction for the troposphere and stratosphere in radio ranging of satellites. – Geophys. Monogr. Ser. **15**, chapter Atmospheric correction for the troposphere and stratosphere in radio ranging of satellites, American Geophysical Union, 247–251.

SAITO, K., T. FUJITA, Y. YAMADA, J. ISHIDA, Y. KUMAGAI, K. ARANAMI, S. OHMORI, R. NAGA-SAWA, S. KUMAGAI, C. MUROI, T. KATO, H. EITO, Y. YAMAZAK, 2006: The operational JMA nonhydrostatic mesoscale model. – Mon. Wea. Rev. **134**, 1266–1298.

STANDARD ATMOSPHERE, U.S., 1976: U.S. Standard Atmosphere 1976. – U.S. Government Printing Office, Washington, D.C.

VEDEL, H., X.-Y. HUANG, 2004: Impact of ground based GPS data on numerical weather prediction. – J. Meteor. Soc. Japan **82**, 459–472.

VEDEL, H., K. SATTLER, 2006: Comparison of TOUGH impact studies with ground-based GPS observations. – TOUGH project deliverable **49**, available at: http://tough.dmi.dk.

WARE, R., C. ALBER, C. ROCKEN, F. SOLHEIM, 1997: Sensing integrated water vapor along GPS ray paths. – Geophys. Res. Lett. **24**, 417–420.

WICKERT, J., G. GENDT, 2006: Fernerkundung der Erdatmosphäre mit GPS. – promet **32**, 176–184.

WULFMEYER, V., H.-S. BAUER, S. CREWELL, G. EHRET, O. REITEBUCH, C. WERNER, M. WIRTH, D. ENGELBART, A. RHODIN, W. WERGEN, A. GIESEN, H. GRASSL, G. HUBER, H. KLINGENBERG, P. MAHNKE, U. KUMMER, C. WÜHRER, P. RITTER, R. WALLENSTEIN, U. WANDINGER, 2003: Lidar research network water vapor and wind. – Meteorol. Z. **12**, 5–24.

WULFMEYER, V., H.-S. BAUER, M. GRZESCHIK, A. BEHRENDT, F. VANDENBERGHE, E. BROWELL, S. ISMAIL, R. FERRARE, 2006: Four-dimensional variational assimilation of water vapor differential absorption lidar data: The first case study within IHOP_2002. – Mon. Wea. Rev. **134**, 209–230.

WULFMEYER, V., A. BEHRENDT, H. S. BAUER, C. KOTTMEIER, U. CORSMEIER, G. ADRIAN, A. BLYTH, G. CRAIG, U. SCHUMANN, M. HAGEN, S. CREWELL, P. D. GIROLAMO, C. FLAMANT, M. MILLER, A. MONTANI, S. MOBBS, E. RICHARD, M. ROTACH, M. ARPAGAUS, H. RUSSCHENBERG, P. SCHLÜSSEL, M. KÖNIG, V. GÄRTNER, R. STEINACKER, M. DORNINGER, D. TURNER, T. WECKWERTH, A. HENSE, C. SIMMER, 2008: The convective and orographically-induced precipitation study: A research and development project of the world weather research program for improving quantitative precipitation forecasting in low-mountain regions. – Bull. Amer. Meteor. Soc. **89**, 1477–1486, DOI:10.1175/2008BAMS2367.1.

XIAO, Q., Y.-H. KUO, J. SUN, W.-C. LEE, E. LIM, Y.-R. GUO, D. M. BARKER, 2005: Assimilation of doppler radar observations with a regional 3D-Var system: Impact of doppler velocities on forecasts of a heavy rainfall case. – J. Appl. Meteor. **44**, 768–788.

ZÄNGL, G., 2002: An improved method for computing horizontal diffusion in a sigma-coordinate model and its application to simulations over mountainous topography. – Mon. Wea. Rev. **130**, 1423–1432.

—, 2004a: Numerical errors above steep topography: A model intercomparison. – Meteorol. Z. **13**, 69–76.

—, 2004b: Numerical simulation of the 12-13 August 2002 flooding event in eastern germany. – Quart. J. Roy. Meteor. Soc. **130**, 1921–1940.

—, 2004c: The sensitivity of simulated orographic precipitation to model components other than cloud microphysics. – Quart. J. Roy. Meteor. Soc. **130**, 1857–1875.

ZOU, X., Y.-H. KUO, Y.-R. GUO, 1995: Assimilation of atmospheric radio refractivity using a nonhydrostatic adjoint model. – Mon. Wea. Rev. **123**, 2229–2249.

ZOU, X., F. VANDENBERGHE, M. PONDECA, Y.-H. KUO, 1997: Introduction to adjoint techniques and the MM5 adjoint modeling system. – Technical report, NCAR Tech. Note NCAR/TN-435-STR, NCAR, P.O. Box 3000, Boulder, CO, 80307.

ZUPANSKI, D., 1993: The effects of discontinuities in the Betts Miller cumulus convective scheme on four-dimensional variational data assimilation. – Tellus A **45**, 511–524.